Brief Communications

# An Asymmetric Increase in Inhibitory Synapse Number Underlies the Development of a Direction Selective Circuit in the Retina

**Ryan D. Morrie**[1] **and Marla B. Feller**[1,2]

[1]Department of Molecular and Cell Biology, and [2]Helen Wills Neuroscience Institute, University of California, Berkeley, Berkeley, California 94720

**Neural circuits rely upon a precise wiring of their component neurons to perform meaningful computations. To compute the direction of motion in the visual scene, the direction selective circuit in the mouse retina depends on an asymmetry in the inhibitory neurotransmission from starburst amacrine cells (SACs) to direction selective ganglion cells (DSGCs). Specifically, depolarization of a SAC on the null side of a DSGC causes a threefold greater unitary inhibitory conductance than depolarization of a SAC on the preferred side. This asymmetry emerges during the second postnatal week of development, but its basis remains unknown. To determine the source of this asymmetry in inhibitory conductance, we conducted paired recordings between SACs and DSGCs at the beginning and end of the second postnatal week. We replaced calcium with strontium to promote asynchronous neurotransmitter release and produce quantal events. During the second postnatal week the quantal frequency but not the quantal amplitude of synaptic events increased more than threefold for null-side SAC-DSGC pairs but remained constant for preferred-side pairs. In addition, paired-pulse depression did not differ between SACs located on the null and preferred sides of DSGCs, indicating that all inhibitory SAC synapses onto a DSGC exhibit the same probability of release. Thus, the higher quantal frequency seen in null-side pairs results from a greater number of inhibitory synapses, revealing that an asymmetry in synapse number between SACs and DSGCs underlies the development of an essential component in the retina's direction selective circuit.**

*Key words:* **asynchronous release; dendrites; GABA; motion; quantal analysis; transgenic mice**

## Introduction

Direction-selective circuits in the mouse retina depend on a precise wiring of inhibitory connections. Retinal direction-selective ganglion cells (DSGCs) respond maximally to stimuli moving in their preferred direction and minimally to stimuli moving in the opposite, or null, direction. This spiking difference results from greater synaptic inhibition onto the DSGC during null-direction motion (Fried et al., 2002; Taylor and Vaney, 2002), whereas the excitatory input is constant regardless of stimulus direction (Yonehara et al., 2013; Park et al., 2014). Several lines of evidence demonstrate that starburst amacrine cells (SACs) are the source of this inhibition. First, eliminating SACs with immunotoxin leads to a loss of direction selectivity (Yoshida et al., 2001). Second, transiently hyperpolarizing SACs reduces direction-selective responses in DSGCs (Vlasits et al., 2014). Third, paired recordings between SACs and DSGCs reveal that SACs located on the null side of a DSGC have a stronger overall inhibitory conductance than those located on the preferred side (Fried et al., 2002; Lee et al., 2010; Wei et al., 2011; Yonehara et al., 2011). Based on a serial EM reconstruction, it has been postulated that the asymmetry in inhibitory input onto DSGCs results from SAC processes pointing in a DSGC's null direction being more likely to form synapses with the DSGC than SAC processes pointing in the preferred direction (Briggman et al., 2011). Yet, when this wiring diagram arises during development is not known. Furthermore, the relative contributions of synaptic strength and functional synapse number to the overall asymmetry in inhibitory synaptic transmission between SACs and DSGCs remain to be determined.

Here we compare the quantal properties of null side versus preferred-side SAC inputs onto DSGCs across the developmental period when asymmetric inhibitory wiring emerges (Wei et al., 2011; Yonehara et al., 2011). We performed paired voltage-clamp recordings from genetically identified DSGCs and SACs under conditions that favor asynchronous release of neurotransmitter and analyzed the quantal properties of events from the null and preferred-side pairs during the second postnatal week. We found that the asymmetric increase in SAC inhibitory synaptic conductance is due, not to a change in release probability or quantal size, but rather to an increase in the number of synapses from null-oriented SAC processes.

## Materials and Methods

*Mice.* To target SACs and posterior-motion preferring DSGCs for recording, we used ChAT-Cre/TdTomato/Drd4 mice generated by crossing together three mouse lines: (1) B6.129S6-ChATtm1(cre)lowl/J (Jackson Laboratories) with Cre driven by the endogenous choline acetyltransferase promoter, (2) B6.129S6-Gt(ROSA)26Sortm9(CAG-td-

Received Feb. 18, 2015; revised May 11, 2015; accepted May 12, 2015.

Author contributions: R.D.M. and M.B.F. designed research; R.D.M. performed research; R.D.M. analyzed data; R.D.M. and M.B.F. wrote the paper.

This work was supported by NIH Grants R01EY019498 and R01EY013528 (M.B.F.) and a NSF Graduate Research Fellowship DGE 1106400 (R.D.M.). We thank P. Han for technical assistance, W. Wei for piloting these studies, and members of the Feller laboratory for commenting on the paper.

The authors declare no competing financial interests.

Correspondence should be addressed to Dr Marla B. Feller, 142 Life Sciences Addition MSC 3200, University of California at Berkeley, Berkeley, CA 94720-3200. E-mail: mfeller@berkeley.edu.

DOI:10.1523/JNEUROSCI.0670-15.2015

 0270-6474/15/359281-06$15.00/0

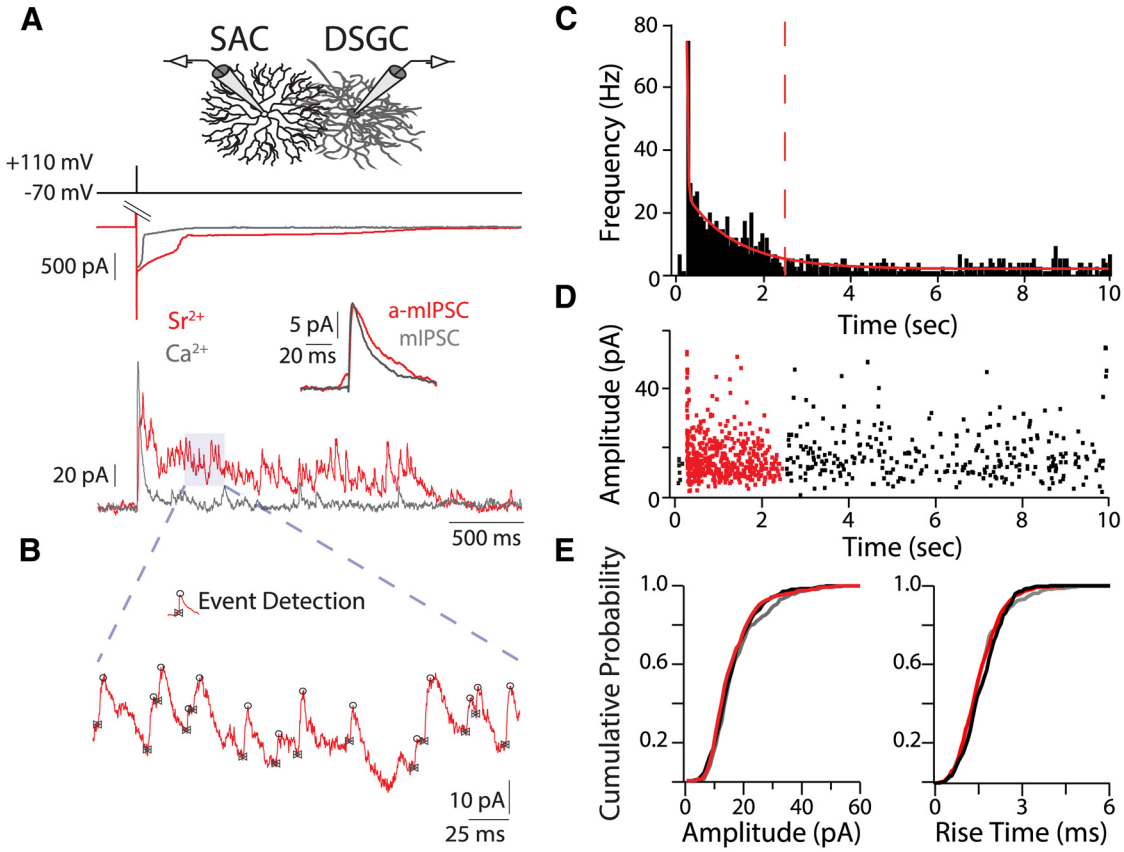


**Figure 1.** Isolation of quantal events from single starburst amacrine cells. ***A***, Voltage-clamp recordings in calcium (gray) and strontium (red) from two different SAC (top traces)-DSGC (bottom traces) pairs show prolonged asynchronous neurotransmitter release from SACs in $Sr^{2+}$-ACSF upon tail current activation. DSGC is held at 0 mV. Inset, Average evoked a-mIPSCs in $Sr^{2+}$-ACSF and average mIPSCs in $Ca^{2+}$-ACSF. ***B***, Example of manual event detection with Taro Tools. IPSC events are marked at their onset (bowties) and peak (circles). ***C***, Frequency histogram (50 ms bins) of IPSC events in $Sr^{2+}$-ACSF for SAC-DSGC pair in ***A***. Stimulus occurred at 250 ms. Solid red line is a double exponential fit to the histogram; dashed red line demarcates a-mIPSCs from mIPSCs (see Materials and Methods). Note: ***C*** and ***D*** display the full 10 s of the sweeps, unlike ***A***. ***D***, Amplitude of IPSCs in $Sr^{2+}$-ACSF for SAC-DSGC pair in ***A***. Red events are a-mIPSCs evoked by a single SAC. Black events are mIPSCs from all SACs. ***E***, Cumulative probability distributions of amplitudes and rise times for a-mIPSCs (red) and mIPSCs (black) in $Sr^{2+}$-ACSF and mIPSCs (gray) in $Ca^{2+}$-ACSF for the SAC-DSGC pairs in ***A***.

Tomato)Hze/J (Jackson Laboratories) with a floxed TdTomato gene, and (3) Tg(Drd4-EGFP)W18Gsat/Mmnc (Mutant Mouse Regional Resource Centers) to label posterior-preferring DSGCs with GFP (Gong et al., 2003; Huberman et al., 2009). All animal procedures were approved by the UC Berkeley Institutional Animal Care and Use Committee and conformed to the NIH *Guide for the Care and Use of Laboratory Animals*, the Public Health Service Policy, and the SFN Policy on the Use of Animals in Neuroscience Research.

*Electrophysiology.* Mice (P7–P14) of either sex were anesthetized with isoflurane and decapitated. Retinas were dissected from enucleated eyes in oxygenated (95% $O_2$/ 5% $CO_2$) $Ca^{2+}$-ACSF containing the following (in mM): 119 NaCl, 2.5 KCl, 1.3 $MgCl_2$, 1 $K_2HPO_4$, 26.2 $NaHCO_3$, 11 D-glucose, and 2.5 $CaCl_2$. Retinal orientation was determined as described previously (Wei et al., 2010). Isolated retinas were cut into dorsal and ventral halves, mounted over a 1–2 $mm^2$ hole in nitrocellulose filter paper (Millipore) with the photoreceptor layer side down, and stored in oxygenated ACSF until use (maximum 8 h).

For quantal recordings, filter paper-mounted retinas were perfused with 30−32°C oxygenated $Sr^{2+}$-ACSF (5 mM $Sr^{2+}$, 2.5 mM EGTA replaces 2.5 mM $Ca^{2+}$) containing the following excitatory synaptic blockers (in μM): 50 AP-5, 20 DNQX, and 10 dihydro-β-erythroidine (Tocris Bioscience). $GFP^+$ and $TdTomato^+$ cells were identified using an epifluorescent microscope (Olympus BX51). The inner limiting membrane above targeted cells was dissected with a glass pipette. Whole-cell voltage-clamp recordings were achieved for a given DSGC before targeting multiple SACs on either side of the DSGC in succession, removing the pipette from the previous SAC before targeting a new SAC. For whole-cell recordings, borosilicate glass capillary tubes pulled to a 4–5 mΩ tip were filled with an internal solution containing the following (in mM): 110 $CsMeSO_3$, 2.8 NaCl, 4 EGTA, 5 TEA-Cl, 4 ATP (magnesium salt), 0.3 GTP (trisodium salt), 20 HEPES, 10 $Na_2$-phosphocreatine, and 0.025 AlexaFluor 488. SACs exhibit asynchronous neurotransmitter release upon depolarization in the voltage-clamp configuration (Fried et al., 2002; Zheng et al., 2004; Lee et al., 2010), which may be at least partially attributed to an inadequate space clamp of the distal neurotransmitter release sites (Miller and Bloomfield, 1983; Zhou, 1998; Hausselt et al., 2007). However, by lowering the $Ca^{2+}$ buffering capacity of the internal solution for SACs (0.1 vs 4 mM EGTA) and using tail currents to elicit responses, we could enhance the synchrony of GABA release from SACs upon depolarization (Fig. 1*A*, gray trace). Due to a lower activation threshold in younger mice P7–P8 SACs were depolarized to 0 mV for 3 ms to induce tail currents. Prolonged tail currents in $Sr^{2+}$-ACSF increased release duration from SACs (Fig. 1*A*, red trace) and may result from a lack of $Ca^{2+}$-dependent inactivation of VGCCs (data not shown).

Paired-pulse recordings were performed in $Ca^{2+}$-ACSF. Although SAC tail currents varied between pulses, IPSCs remained consistent between sweeps (see Fig. 3*A*). $MgCl_2$ replaced $CaCl_2$ when lowering $Ca^{2+}$ concentration (see Fig. 3*C*) to maintain $[Cl^-]_{out}$ and osmolarity.

Data were acquired at 10 kHz and filtered at 2 kHz with a Multiclamp 700B amplifier using pCLAMP 10 recording software and a Digidata 1440 digitizer (Molecular Devices). Reported holding potentials have been corrected for the junction potential (−10 mV). Series resistance (<65 mΩ for all DSGCs) was not compensated, but the current divider

effect of the series resistance, $(R_{series} + R_{input})/R_{input}$, was similar across all recordings (range = 1.05–1.27, SD = 0.049).

*Data analysis.* Data analysis was performed in IgorPro (WaveMetrics) and MATLAB (MathWorks). The Taro Tools (sites.google.com/site/tarotoolsregister/) plug-in for IgorPro was used to detect and analyze quantal events (Fig. 1*B*). Events were detected manually for each trace because some traces had multiple overlapping events, preventing the use of amplitude thresholds for event detection. The decay time parameter was 2.5 ms (default) to separate overlapping events. Frequency, amplitude, rise time, and average event calculations were computed with "Further Analysis" and "Event Cut Out" options. Large (>60 pA) initial IPSCs after SAC stimulation resulting from synchronous neurotransmitter release were excluded from analysis. Frequency histograms were fit with a double exponential (Fig. 1*C*, red line). Evoked asynchronous miniature IPSCs (a-mIPSCs) were separated from spontaneous mIPSCs when the curve reached baseline frequency plus two SD (Fig. 1*C*, red dashed line). Mean a-mIPSC frequency was calculated from 50 to 968 ms poststimulation (the average time when frequency decayed to baseline for p7–8 SAC-DSGC pairs). Frequency measures were normalized by subtracting the baseline mIPSC frequency to isolate a-mIPSCS specific to the depolarized SAC. Paired-pulse ratio was calculated by dividing the amplitude of the second IPSC by the amplitude of the first IPSC after averaging at least three traces for a given interstimulus interval.

## Results

### Presynaptic mechanisms mediate changes in SAC-DSGC connectivity during development

The asymmetry in inhibitory conductance present in the mature direction-selective circuit emerges during the second postnatal week in mice (Wei et al., 2011; Yonehara et al., 2011), but whether it manifests as an increase in synapse strength or synapse number is unknown. Previous recordings have demonstrated that from P7 to P14 mIPSCs measured in DSGCs increase in frequency but not in amplitude (Wei et al., 2011), indicating a presynaptic change in SAC-DSGC connectivity during development. However, it has been estimated that each DSGC can receive inputs from ~35 different SACs distributed on all sides (Keeley et al., 2007), and therefore changes in mIPSC frequency cannot be attributed to null-side SACs alone.

Thus, we first sought to isolate quantal events recorded in DSGCs from single SACs whose somas were located on the null and preferred sides of the DSGC. We conducted paired recordings in solutions in which we replaced $Ca^{2+}$ with $Sr^{2+}$ to increase the asynchronous component of neurotransmitter release and generate IPSCs that are quantal in nature (Goda and Stevens, 1994; Xu-Friedman and Regehr, 1999, 2000). We used brief, strong depolarizations (5 ms, 120 mV) to trigger release from calcium tail currents (Singer and Diamond, 2003; Singer et al., 2004), which led to a primarily synchronous release of neurotransmitter when recordings were performed in $Ca^{2+}$-ACSF (Fig. 1*A*, gray trace). In contrast, depolarization of SACs in $Sr^{2+}$-ACSF induced a prolonged asynchronous release of GABA onto DSGCs (Fig. 1*A*, red trace). During this prolonged release, individual a-mIPSCs evoked from the depolarized SAC could be resolved (Fig. 1*B*; see Materials and Methods). a-mIPSCs were considered quantal events because a-mIPSCs and mIPSCs displayed similar amplitudes and kinetics (Fig. 1*D*,*E*).

To determine whether a presynaptic or postsynaptic change in SAC-DSGC synapses produces the asymmetry in inhibitory conductance, we analyzed the frequency and amplitude of a-mIPSCs evoked from SACs located on the null and preferred sides of DSGCs (Fig. 2*A*). At P7–P8, null and preferred-side pairs displayed similar a-mIPSC frequencies and amplitudes (Fig. 2*B*,*C*; $n = 5$ DSGCs, 6 null SACs, 5 preferred SACs), consistent with the

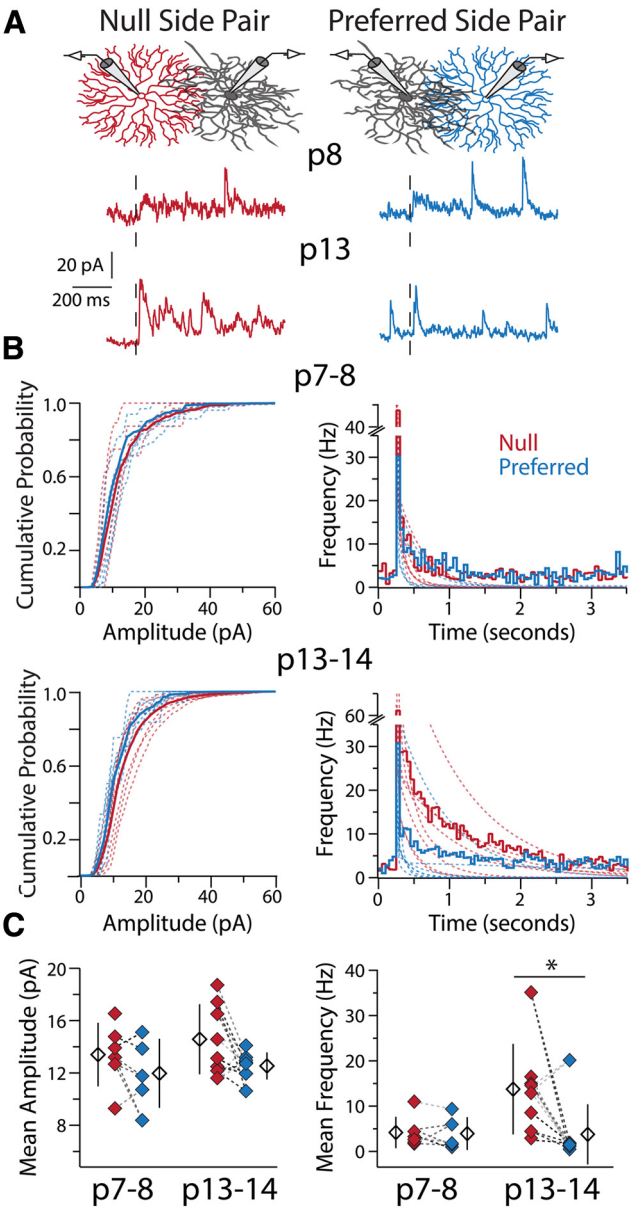


**Figure 2.** Presynaptic mechanisms underlie the changes in SAC-DSGC connectivity during development. ***A***, Example recordings in $Sr^{2+}$-ACSF from two DSGCs at different ages upon stimulation (black dashed line) of a null- and a preferred-side SAC connected to each DSGC. Stimulation of the null-side SAC at P13 produces a greater frequency of a-mIPSCs. ***B***, Average cumulative probability distributions of a-mIPSC amplitudes (left) and average peristimulus frequency histograms (right) for null and preferred-side pairs at P7–P8 (top) and P13–P14 (bottom). Dashed lines are cumulative probability distributions of a-mIPSC amplitudes or double-exponential fits to frequency histograms (as per Fig. 1*C*) for individual pairs. ***C***, Mean a-mIPSC amplitude (left) and mean a-mIPSC frequency (right; see Materials and Methods) for each SAC-DSGC pair. Amplitude and frequency measures recorded in the same DSGC for preferred- and null-side pairs are connected via dashed lines of the same color. Average a-mIPSC amplitudes are not significantly different between groups (one-way ANOVA, $p = 0.18$, df = 26), whereas a-mIPSC frequency is significantly different at P13–P14, but not P7–P8, between null- and preferred-side pairs (Kruskal–Wallis one-way ANOVA, $p = 0.006$, df = 3; Dunn-Holland-Wolfe *post hoc*, $p = 0.007$; Null P13–P14 vs Pref P13–P14). Note, the one preferred-side SAC-DSGC pair with a high a-mIPSC frequency was the only SAC-DSGC pair in this study with an intersoma distance of <50 $\mu$m (see Discussion). Open diamonds are population averages, error bars show SD, and asterisk highlights significant difference between groups for this and all subsequent figures.

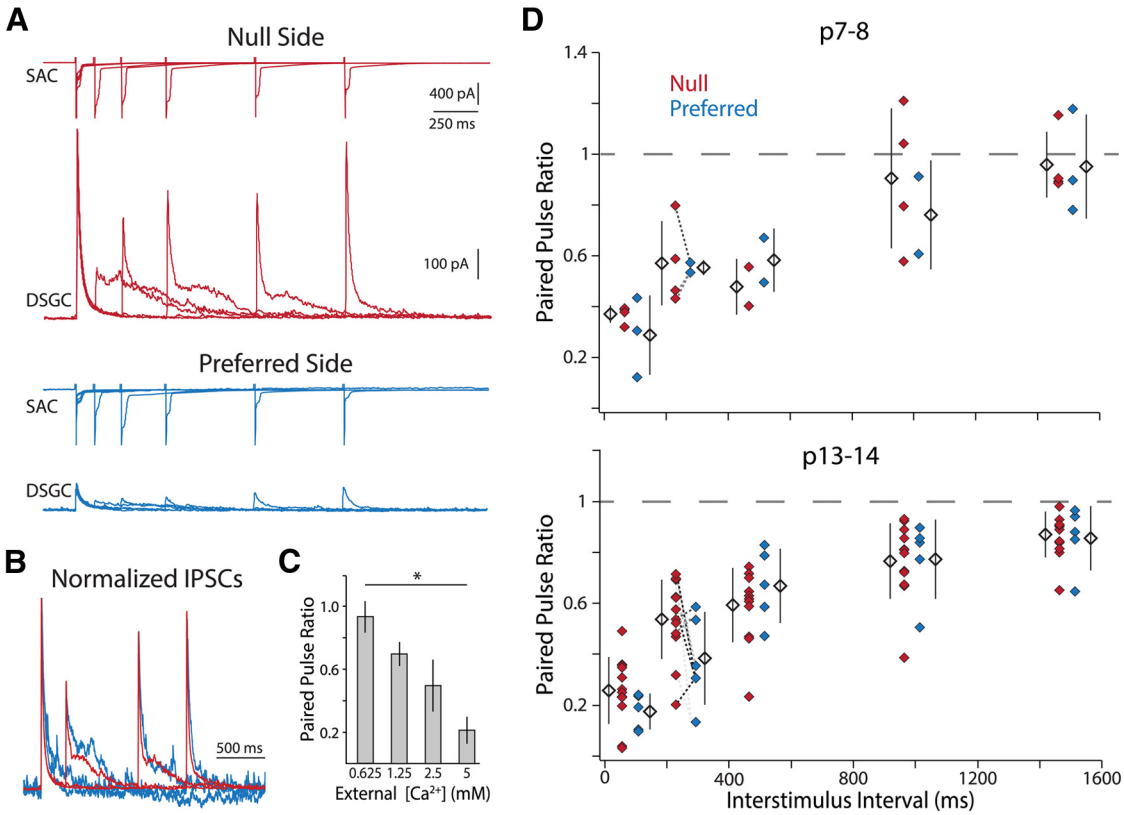


**Figure 3.** Null- and preferred-side SAC-DSGC synapses display similar paired-pulse depression throughout development. ***A***, Example traces from paired-pulse protocol. Top traces of each color show tail currents elicited from a null (red) and a preferred side (blue) P14 SAC at varying interstimulus time intervals (100, 250, 500, 1000, 1500 ms) in $Ca^{2+}$-ACSF. Bottom traces show responses of their shared postsynaptic DSGC held at 0 mV. ***B***, IPSCs evoked from preferred- and null-side SACs display the same kinetics. Peak normalized traces from ***A*** for 250, 1000, and 1500 ms interstimulus intervals. ***C***, The average paired-pulse ratio for P13–P14 SAC-DSGC pairs decreases as external $Ca^{2+}$ increases for the 250 ms interstimulus interval. All groups are significantly different from each other (one-way ANOVA, $p = 2.2 \times 10^{-9}$, df = 35; Tukey-Kramer *post hoc*, $p < 0.05$). ***D***, Paired-pulse ratio at the beginning and end of the second postnatal week as a function of interstimulus interval. Data points for the 250 ms interstimulus interval recorded in the same DSGC are connected via dashed lines of the same color.

similar inhibitory currents observed at this point in development (Wei et al., 2011; Yonehara et al., 2011). By P13–P14 the average a-mIPSC frequency was >3 times greater for null-side pairs than preferred-side pairs (Fig. 2*B*,*C*; $n = 5$ DSGCs, 8 null SACs, 8 preferred SACs), matching the previously observed asymmetry in overall inhibitory conductance (Wei et al., 2011). Null-side pairs also trended toward having larger a-mIPSC amplitudes at this age, but this difference was not significant (Fig. 2*B*,*C*). Therefore, the asymmetry in inhibitory conductance emerges via a presynaptic mechanism at null-side SAC-DSGC synapses, with postsynaptic mechanisms (e.g., increases in $GABA_AR$ expression per synapse) at most a minor contributor to the development of asymmetric inhibitory input.

### Null- and preferred-side SACs exhibit similar paired-pulse depression throughout development

The asymmetric increase in a-mIPSC frequency during development indicates that either null-side SACs form more synapses with DSGCs or that synapses from null-side SACs increase their probability of vesicle release during the second postnatal week. To distinguish between these possibilities, we performed paired-pulse recordings with SAC-DSGC pairs in $Ca^{2+}$-ACSF (Fig. 3*A*). Importantly, our paired-pulse ratio altered inversely with external $Ca^{2+}$ concentration, demonstrating reliability in our measure of relative vesicle release probability via tail currents (Singer et al., 2004; Fig. 3*C*; for each $[Ca^{2+}]$ in mM: 0.625, $n = 3$ DSGCs, 7 pairs; 1.25, $n = 3$ DSGCs, 6 pairs; 2.5, $n = 6$ DSGCs, 14 pairs; 5.0, $n = 2$ DSGCs, 5 pairs). Paired-pulse recordings of SAC-DSGC pairs at the beginning and end of the second postnatal week showed the average paired-pulse ratio did not differ between null- and preferred-side pairs at either age, or between pairs at different ages (Fig. 3*D*; P7–P8, $n = 4$ DSGCs, 4 null SACs, 3 preferred SACs; P13–P14, 6 DSGCs, 12 null SACs, 5 preferred SACs). Thus the asymmetric increase in a-mIPSC frequency (Fig. 2) is not due to an increase in vesicle release probability, but is rather a result of null-side SACs forming more synapses onto DSGCs from P7–P14.

### Null-side SACs form synapses closer to the DSGC soma

It has been suggested that null-oriented SAC processes (Fig. 4*A*, red shading) are more likely to form synapses with DSGCs than preferred oriented SAC processes, regardless of SAC somatic location relative to the DSGC (Briggman et al., 2011). This would lead to the following synaptic configuration: for null-side pairs the null-oriented SAC processes overlap extensively with the DSGC dendrites (form synapses at proximal and distal locations), whereas for preferred-side pairs, the null-oriented SAC processes only overlap, and thus only form synapses, with DSGC dendrites at very distal locations (Fig. 4*A*). This proposed arrangement would result in increased dendritic filtering of synaptic events from preferred-side SACs, prolonging the rise times of synaptic events when recording at the DSGC soma (Rall, 1967).

To test for this scenario physiologically, we analyzed the average a-mIPSC rise times for null- and preferred-side pairs at P13–

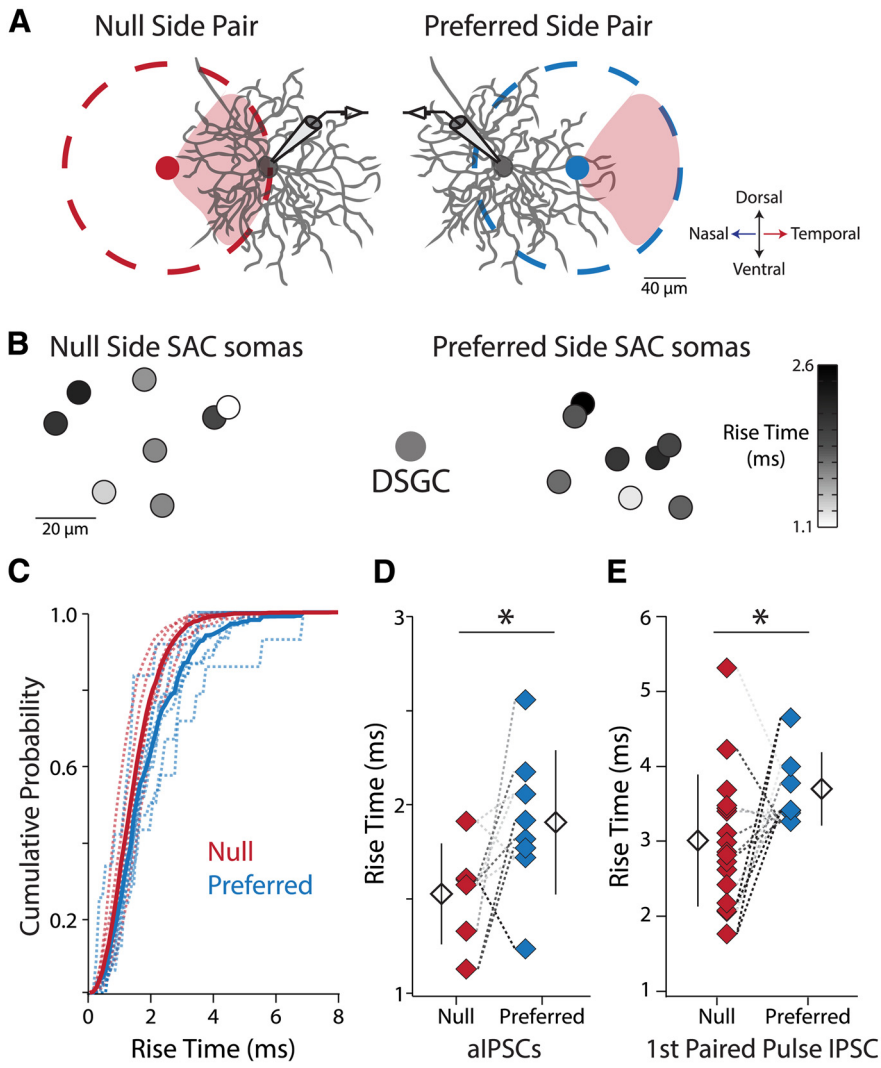


**Figure 4.** Synapses from null-side SACs are located closer to the DSGC soma than synapses from preferred-side SACs at P13–P14. ***A***, Model in which SAC-DSGC synapses are located where the DSGC's dendrites overlap with the portion of the SAC dendritic arbor (dashed circles) oriented in the DSGC's null direction (red shading, temporal retinal direction for Drd4-GFP $^{+}$ cells; Briggman et al., 2011). The null-oriented portion of the null-side SAC's dendritic arbor overlaps extensively with the DSGC's dendrites at both proximal and distal locations. In contrast, the null-oriented portion of the preferred-side SAC's dendritic arbor only overlaps with DSGC dendrites at very distal locations. Thus, upon depolarization of the preferred-side SAC signals from synaptic events will experience greater dendritic filtering when recording at the DSGC soma. All diagrams are to scale based on average dendritic arbor size at P14 (Wei et al., 2011) but note that DRD4-GFP $^{+}$ cells often have asymmetric dendritic fields (Rivlin-Etzion et al., 2011). Null- and preferred-side SAC somata are located 89 and 70 $\mu$m away from the DSGC soma respectively, the average intersoma distance for the two groups at P13–P14. ***B***, Heat map of average a-mIPSC rise times. Small circles are SAC soma locations relative to the DSGC soma. Null-side SACs close to the DSGC have the fastest rise times, whereas preferred-side SACs the same distance away have slower rise times. ***C***, Average cumulative probability distributions of 10–90% a-mIPSC rise times for null-side and preferred-side SAC-DSGC pairs with intersoma distances $<100$ $\mu$m (6 null-side pairs, 8 preferred-side pairs). Dashed lines are cumulative probability distributions for individual pairs. ***D***, Average 10–90% a-mIPSC rise times for SAC-DSGC pairs in ***C*** (Welch's *t* test, $p = 0.049$, df $= 11.98$). ***E***, Average 10–90% IPSC rise times for SAC-DSGC pairs for the initial IPSCs in the paired-pulse protocol (Fig. 2*A*; Welch's *t* test, $p = 0.025$, df $= 19.5$). Rise times measured from the same DSGC are connected via dashed lines of the same color for ***D*** and ***E***.

P14 (Fig. 4*B*). To ensure the same overall degree of SAC-DSGC dendritic overlap between null- and preferred-side pairs, we statistically compared the rise times of null- and preferred-side SAC-DSGC pairs with intersoma distances $<100$ $\mu$m. We found that the distribution of a-mIPSC rise times for preferred-side pairs is shifted to higher values than the distribution for null-side pairs (Fig. 4*C*; $n = 5$ DSGCs, 6 null SACs, 8 preferred SACs). This shift in the distribution is reflected in significantly longer average a-mIPSC rise times for preferred-side pairs than null-side pairs (Fig. 4*D*). Furthermore, this effect was also present in $Ca^{2+}$-ACSF, where the average rise times for the initial IPSCs in the paired-pulse protocol were longer for preferred-side pairs than null-side pairs (Fig. 4*E*; $n = 10$ DSGCs, 17 null SACs, 7 preferred SACs). Thus, our data are consistent with a model in which, by P13–P14, SAC-DSGC synapses are primarily located at sites of overlap between DSGC dendrites and null-oriented SAC processes. From our findings, we conclude that during the second postnatal week, null-oriented SAC processes form more synapses with DSGCs than preferred oriented SAC processes, establishing the asymmetry in inhibitory conductance required for direction selectivity.

## Discussion

By comparing the properties of quantal events in DSGCs from null- and preferred-side SACs during the second postnatal week, we have found that quantal event frequency, but not amplitude, dramatically increases solely for null-side SAC-DSGC pairs. We have also demonstrated that SAC-DSGC synapses are usually found at sites of overlap with null-oriented SAC processes and all exhibit similar probabilities of release. Thus, we conclude that during development there is a specific increase in functional inhibitory synapse number from null-oriented SAC processes to DSGCs. Our results provide the first unambiguous and physiological explanation for the development of the asymmetric inhibitory conductance required for direction selectivity in the mouse retina.

A model in which synapses are formed at sites of overlap between null oriented SAC processes and DSGC dendrites also provides an explanation for the lone preferred-side SAC-DSGC pair with a high a-mIPSC frequency (Fig. 2*C*; 20.2 Hz). This preferred-side SAC was the only depolarized SAC located within 50 $\mu$m of a DSGC, allowing extensive overlap of its null-oriented processes with the dendritic arbor of the DSGC, despite the preferred-side somatic location. When we recorded from this same DSGC while depolarizing a preferred-side SAC further away (67 $\mu$m), the average a-mIPSC frequency dropped to 1.4 Hz (Fig. 2*C*), as this more distant SAC had many fewer null-oriented processes overlapping with the DSGC's dendrites.

The present study identifies synapse formation from null-oriented processes as the driving force behind the development of retinal direction selectivity. However, how this specificity is achieved remains unresolved. SAC-DSGC connectivity is hypothesized to be hard-wired, relying on each of the four classes of ON–OFF DSGCs to express a particular synaptogenic marker

whereas complimentary markers are expressed on SAC processes oriented in the null direction (Elstrott and Feller, 2009). If different SAC processes do express different synaptogenic factors during a specified time in development, how each SAC robustly achieves this expression pattern remains to be determined. Interestingly, from P7–P14 SAC processes grow extensively and develop varicosities (Zheng et al., 2004; Wei et al., 2011), the sites of neurotransmitter release (Famiglietti, 1991; Briggman et al., 2011). Analyzing the emergence and interactions of these structures with DSGC dendrites during development may provide insight into the preferential association of DSGCs with null-oriented SAC processes. Thus, the retinal direction-selective circuit will continue to enhance our understanding of the mechanisms underlying inhibitory circuit development.

## References


Briggman KL, Helmstaedter M, Denk W (2011) Wiring specificity in the direction-selectivity circuit of the retina. Nature 471:183–188. CrossRef Medline

Elstrott J, Feller MB (2009) Vision and the establishment of direction-selectivity: a tale of two circuits. Curr Opin Neurobiol 19:293–297. CrossRef Medline

Famiglietti EV (1991) Synaptic organization of starburst amacrine cells in rabbit retina: analysis of serial thin sections by electron microscopy and graphic reconstruction. J Comp Neurol 309:40–70. CrossRef Medline

Fried SI, Münch TA, Werblin FS (2002) Mechanisms and circuitry underlying directional selectivity in the retina. Nature 420:411–414. CrossRef Medline

Goda Y, Stevens CF (1994) Two components of transmitter release at a central synapse. Proc Natl Acad Sci U S A 91:12942–12946. CrossRef Medline

Gong S, Zheng C, Doughty ML, Losos K, Didkovsky N, Schambra UB, Nowak NJ, Joyner A, Leblanc G, Hatten ME, Heintz N (2003) A gene expression atlas of the central nervous system based on bacterial artificial chromosomes. Nature 425:917–925. CrossRef Medline

Hausselt SE, Euler T, Detwiler PB, Denk W (2007) A dendrite-autonomous mechanism for direction selectivity in retinal starburst amacrine cells. Plos Biol 5:e185. CrossRef Medline

Huberman AD, Wei W, Elstrott J, Stafford BK, Feller MB, Barres BA (2009) Genetic identification of an on–off direction-selective retinal ganglion cell subtype reveals a layer-specific subcortical map of posterior motion. Neuron 62:327–334. CrossRef Medline

Keeley PW, Whitney IE, Raven MA, Reese BE (2007) Dendritic spread and functional coverage of starburst amacrine cells. J Comp Neurol 505:539–546. CrossRef Medline

Lee S, Kim K, Zhou ZJ (2010) Role of ACh-GABA cotransmission in detecting image motion and motion direction. Neuron 68:1159–1172. CrossRef Medline

Miller RF, Bloomfield SA (1983) Electroanatomy of a unique amacrine cell in the rabbit retina. Proc Natl Acad Sci U S A 80:3069–3073. CrossRef Medline

Park SJ, Kim IJ, Looger LL, Demb JB, Borghuis BG (2014) Excitatory synaptic inputs to mouse on–off direction-selective retinal ganglion cells lack direction tuning. J Neurosci 34:3976–3981. CrossRef Medline

Rall W (1967) Distinguishing theoretical synaptic potentials computed for different soma-dendritic distributions of synaptic input. J Neurophysiol 30:1138–1168. Medline

Rivlin-Etzion M, Zhou K, Wei W, Elstrott J, Nguyen PL, Barres BA, Huberman AD, Feller MB (2011) Transgenic mice reveal unexpected diversity of on–off direction-selective retinal ganglion cell subtypes and brain structures involved in motion processing. J Neurosci 31:8760–8769. CrossRef Medline

Singer JH, Diamond JS (2003) Sustained Ca2+ entry elicits transient postsynaptic currents at a retinal ribbon synapse. J Neurosci 23:10923–10933. Medline

Singer JH, Lassová L, Vardi N, Diamond JS (2004) Coordinated multivesicular release at a mammalian ribbon synapse. Nat Neurosci 7:826–833. CrossRef Medline

Taylor WR, Vaney DI (2002) Diverse synaptic mechanisms generate direction selectivity in the rabbit retina. J Neurosci 22:7712–7720. Medline

Vlasits AL, Bos R, Morrie RD, Fortuny C, Flannery JG, Feller MB, Rivlin-Etzion M (2014) Visual stimulation switches the polarity of excitatory input to starburst amacrine cells. Neuron 83:1172–1184. CrossRef Medline

Wei W, Elstrott J, Feller MB (2010) Two-photon targeted recording of GFP-expressing neurons for light responses and live-cell imaging in the mouse retina. Nat Protoc 5:1347–1352. CrossRef Medline

Wei W, Hamby AM, Zhou K, Feller MB (2011) Development of asymmetric inhibition underlying direction selectivity in the retina. Nature 469:402–406. CrossRef Medline

Xu-Friedman MA, Regehr WG (1999) Presynaptic strontium dynamics and synaptic transmission. Biophys J 76:2029–2042. CrossRef Medline

Xu-Friedman MA, Regehr WG (2000) Probing fundamental aspects of synaptic transmission with strontium. J Neurosci 20:4414–4422. Medline

Yonehara K, Balint K, Noda M, Nagel G, Bamberg E, Roska B (2011) Spatially asymmetric reorganization of inhibition establishes a motion-sensitive circuit. Nature 469:407–410. CrossRef Medline

Yonehara K, Farrow K, Ghanem A, Hillier D, Balint K, Teixeira M, Jüttner J, Noda M, Neve RL, Conzelmann KK, Roska B (2013) The first stage of cardinal direction selectivity is localized to the dendrites of retinal ganglion cells. Neuron 79:1078–1085. CrossRef Medline

Yoshida K, Watanabe D, Ishikane H, Tachibana M, Pastan I, Nakanishi S (2001) A key role of starburst amacrine cells in originating retinal directional selectivity and optokinetic eye movement. Neuron 30:771–780. CrossRef Medline

Zheng JJ, Lee S, Zhou ZJ (2004) A developmental switch in the excitability and function of the starburst network in the mammalian retina. Neuron 44:851–864. CrossRef Medline

Zhou ZJ (1998) Direct participation of starburst amacrine cells in spontaneous rhythmic activities in the developing mammalian retina. J Neurosci 18:4155–4165. Medline